G Model
GEOD-1161; No. of Pages 10
ARTICLE IN PRESS
Journal of Geodynamics xxx (2012) xxx–xxx

Contents lists available at SciVerse ScienceDirect

Journal of Geodynamics

journal homepage: http://www.elsevier.com/locate/jog

Kinematic study at the junction of the East Anatolian fault and the Dead Sea fault from GPS measurements

Yasser Mahmoud[a,*], Frederic Masson[a], Mustapha Meghraoui[a], Ziyadin Cakir[b], Abdulmutaleb Alchalbi[c], Hakan Yavasoglu[d], Onder Yönlü[e], Mohamed Daoud[c], Semih Ergintav[f], Sedat Inan[f]

[a] IPGS, CNRS/University of Strasbourg, France
[b] Department of Geology, Istanbul Technical University, Turkey
[c] NEC-Syrian National Earthquake Center, Damascus, Syria
[d] Department of Geomatics, Istanbul Technical University, Turkey
[e] Department of Geology, Eskisehir Osmangazi University, Turkey
[f] TUBITAK, Marmara Research Center, Gebze, Turkey

ARTICLE INFO

Article history:
Received 6 June 2011
Received in revised form 27 January 2012
Accepted 8 May 2012
Available online xxx

Keywords:
Dead Sea fault zone
East Anatolian fault zone
GPS
Velocity rate
Active tectonics

ABSTRACT

The Hatay Triple Junction (HTJ) is a tectonically complex area located at the intersection between the left-lateral East Anatolian fault (EAF), the Cyprus subduction arc and the left-lateral Dead Sea fault (DSF) which is a transform boundary between the Arabian and Sinai plates as they converge toward Eurasia. Previous GPS studies indicate a left-lateral strike-slip rate across the DSF varying from 5 mm/yr (along the southern part) to 2 mm/yr (along the northern part) (Alchalbi et al., 2010; Gomez et al., 2007; Le Béon et al., 2008; Mahmoud et al., 2005; Al-Tarazi et al., 2011). In contrast, the EAF has a roughly constant velocity along strike estimated at 9.7 + 0.9 mm/yr (Reilinger et al., 2006). The HTJ contains several well-identified active fault segments (DSF, EAF, Osmaniye fault, Karasu fault, Latakia fault, Jisr-al-shuggur fault, Idleb fault and Afrin fault) (Meghraoui et al., 2011), the fault-slip rates for which are poorly constrained.

In order to constrain better the slip rate on faults, we established a network of 57 GPS sites in NW Syria and in SE Turkey. The first campaign was carried out in September 2009; a second took place in September and November 2010 and a third (only in Turkey) in September 2011. Although the velocity field vectors computed from the 2009, 2010 and 2011 measurements appear consistent with other local studies, the results are hampered by large uncertainties due to the short observation period. However, preliminary interpretations are consistent with decreasing velocity along the DSF from south to north reported previously.

1. Introduction

The intersection between the Dead Sea fault (DSF), East Anatolian fault (EAF) and Cyprus arc corresponds to the Hatay Triple Junction (HTJ) in south-eastern Turkey and north-western Syria (Fig. 1) forming the plate boundaries between Arabia, Africa and Anatolia (Jackson and McKenzie, 1988). The Hatay tectonic zone is among the few Fault-Fault-Trench (FFT) triple junctions. Other comparable FFT triple junctions are the Mendocino (North America-Pacific-Juan de Fuca plates) and the Kamchatka-Aleutian (Eurasia-Okhotsk-North America plates) that are mainly in oceanic domains (Furlong, 1984; Kozhurin, 2007; McKenzie and Morgan, 1969). The HTJ has the unique advantage to be partly intracontinental and offers a visible and accessible intersection between the EAF, the DSF and the Cyprus subduction zone. Recently, GPS studies provide 18 ± 2 mm/yr for the north-westward motion of Arabia toward Eurasia and 6 ± 2 mm/yr for the northward motion of Africa toward Eurasia in the eastern Mediterranean (Reilinger et al., 2006). At a large scale, the junction is at the intersection between the EAF, DSF and the Cyprus arc with its inland continuation, the Karasu Valley Fault (KVF) in southern Turkey and northern Syria (Meghraoui et al., 2011). The active deformation and related block tectonics in the vicinity of the TJ are, however, poorly constrained and a better assessment of fault strain accumulation rate and interseismic behavior are needed in the HTJ.

The junction appears nowadays as a zone of diffuse and low-level seismicity but the presence of major active strike-slip faults and cumulative offsets (Altunel et al., 2009; Karabacak et al., 2010; Meghraoui et al., 2011) suggests the occurrence of large

* Corresponding author.
E-mail addresses: yasser.mahmoud@eost.u-strasbg.fr, yasser@unistra.fr (Y. Mahmoud).

0264-3707/$ – see front matter © 2012 Elsevier Ltd. All rights reserved.
http://dx.doi.org/10.1016/j.jog.2012.05.006

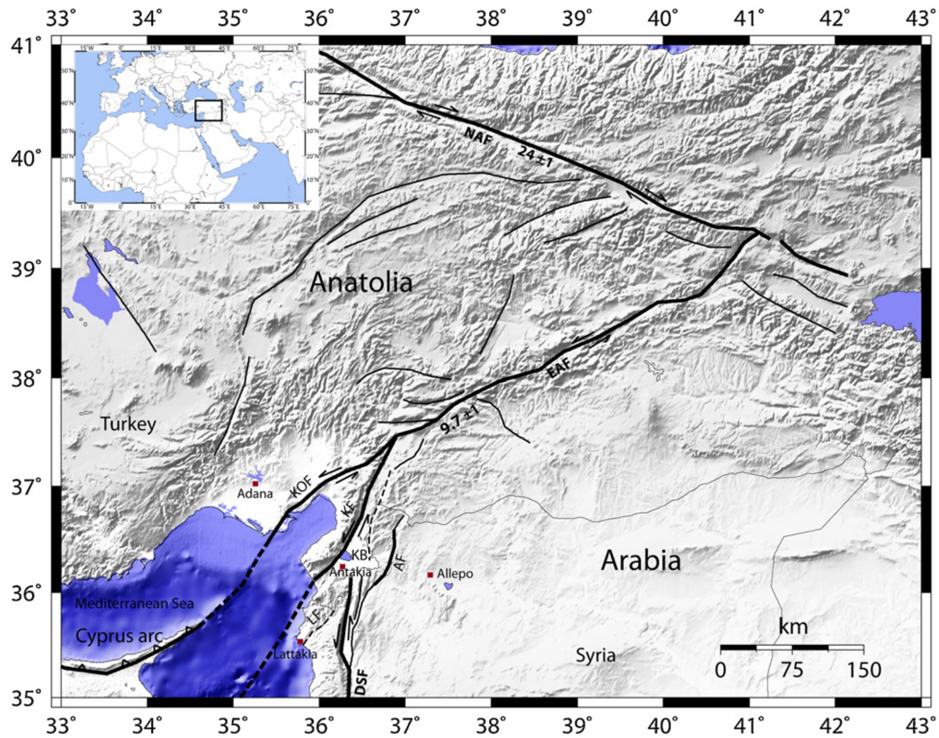

Fig. 1. Map showing the Hatay triple junction area and the principal faults in the region (Meghraoui et al., 2011). The key tectonic features: AGF: Al Ghab fault, AF: Afrin fault, CA: Cyprus Arc, DSF: Dead sea fault, KB: Karasu basin, KF: Karasu fault, KOF: Karatas-Osmaniye fault, LF: Lattakia fault, MF: Missyaf fault, NAF: north Anatolian fault, EAF: East Anatolian fault.

earthquakes with coseismic rupture displacements. Indeed, the HTJ has been the site of numerous historical earthquakes, where in particular the largest seismic event occurred on 19 November 1114 (M 7.8) along the EAF, 29 December 1408 (M 7.4) along the DSF and 13 August 1822 (M 7.3) along the Karasu Fault (Ambraseys and Jackson, 1998; Sbeinati et al., 2005; Sbeinati, 2010). The M_w 6.2 Adana earthquake of 1998 near the EAF (Aktar et al., 2000) and the M_w 6.8 Cyprus subduction zone earthquake of 1996 (Papazachos and Papaioannou, 1999) also attest to the occurrence of large earthquakes more recently. The junction "sensu stricto" was relatively quiescent during the last century, but its late Quaternary tectonics, historical seismic activity and geodetic studies indicate the possibility of a significant seismic strain release (Altunel et al., 2009; Ambraseys and Jackson, 1998; Meghraoui et al., 2003; Salamon et al., 2003; Sbeinati et al., 2005).

In this paper, we present a kinematic synthesis of the active tectonics of the HTJ and compare with the previous geodetic rates, reported along faults comprising this complex junction. A new GPS network that consists in four profiles across the DSF, the EAF and Karasu Valley Fault has been installed and measured and is expected to provide better constraints of the active deformation at the HTJ. After data processing and analysis, we present new results and discuss their consistency with previous tectonic and geodetic studies of the region.

2. Kinematic synthesis of the DSF

Recent studies have characterized the first order geodetic velocity field around the DSF (Alchalbi et al., 2010; Gomez et al., 2007; Le Béon et al., 2008; Reilinger et al., 2006; Al-Tarazi et al., 2011). These separate velocity fields have been individually combined applying rotational transformations, which minimize the residual misfit of GPS velocities for the sites that are common to Reilinger et al. (2006), in order to apply the rotational transformation we used (12) common sites from Alchalbi et al. (2010) and Gomez et al. (2007), (12) common sites from Le Béon et al. (2008) and (16) common sites from Al-Tarazi et al. (2011), the RMSs fit for these transformations are 0.66 mm/yr, 0.48 mm/yr and 0.2 mm/yr, respectively. Part of the combined data is shown in Fig. 2a in an Arabia fixed reference frame. Following (Savage and Burford, 1973), using 1-D elastic dislocation model of a locked fault assumes an infinitely long strike-slip fault and expresses the station velocity, b, as a function of the long-term slip rate (V), fault locking depth (D) and distance from the fault (x):

$$b = \left(\frac{V}{\pi}\right) \arctan\left(\frac{x}{D}\right) \tag{1}$$

From this relationship, it is possible to estimate the relative movement of the Africa-Sinai block compared to Arabia using a simple block model. Assuming a single fault with uniform slip along strike, this results in a rate of strain accumulation for the DSF of $\sim 4.5 \pm 0.3$ mm/yr (Reilinger et al., 2006).

However, more detailed information of the velocity field confirms that the velocity is varying along strike. From a rate of about 4.5 mm/yr along the southern and central segments (Mahmoud et al., 2005) to a rate of about 2 mm/yr along the northern segment (north of 35°; Alchalbi et al., 2010). Moreover all the profiles across the fault (Fig. 2b), central or north do not have a density of points and/or measurement accuracy sufficient to allow unambiguous determination of the locking depth of the fault. A locking depth of 11 ± 9 km is proposed along the southernmost segment (Le Béon et al., 2008) while this looking depth is very difficult to estimate along the northernmost segment (Alchalbi et al., 2010).

The slip rate of $\sim$4.5 mm/yr proposed along the southern and central parts of the DSF is consistent with 1000–1300 yr mean return periods for strike-slip earthquakes within the Lebanese

Please cite this article in press as: Mahmoud, Y., et al., Kinematic study at the junction of the East Anatolian fault and the Dead Sea fault from GPS measurements. J. Geodyn. (2012), http://dx.doi.org/10.1016/j.jog.2012.05.006

restraining bend (Daeron et al., 2007; Gomez et al., 2003; Nemer et al., 2008) and along the southern DSF segment (Ferry et al., 2007; Klinger et al., 2000a). They are also consistent with paleoseimological and geomorphological studies (Ambraseys et al., 1994; Freund, 1970; Ginat et al., 1998; Guidoboni et al., 1994; Klinger et al., 2000a, 2000b; Niemi et al., 2001; Zilberman et al., 2005; Ferry et al., 2011). Conversely, the very low velocity observed along the northern segment is not consistent with long-term rates (Meghraoui et al., 2003; Sbeinati et al., 2010) and is not easily integrated into a regional kinematic model of the HTJ.

3. Geodetic data around the HTJ

GPS campaigns using Trimble 4000SSI, 4000SSE, 4700, 5700 and Ashtech UZ12 were initiated in Hatay province in 1991 and observed again in 1994, 1996, 1998, 2002 and 2004. Fig. 5 shows the location of the 22 GPS sites and the velocities from Reilinger et al. (2006) computed for an Arabia fixed reference frame. The GPS stations were re-measured in 2004 in conjunction with the Massachusetts Institute of Technology, with Strasbourg participation supported in the frame of the EC-Funded project APAME (Meghraoui et al., 2011).

Although stations located on the Arabian plate show negligible movements, Anatolia exhibits a south-westward movement with a maximum velocity of 10.2 ± 1.6 mm/yr at ANDR station (Fig. 5). To the southwest, GPS velocities at DORT, ISKE, ULUC and ULCN show similar directions with stations north of the EAF and they seem to belong to the Anatolian plate. However, their reduced velocities (4.5–5.8 mm/yr) which are about half of those of the Anatolian plate and left-lateral slip of the EAF, imply a significant fault slip and

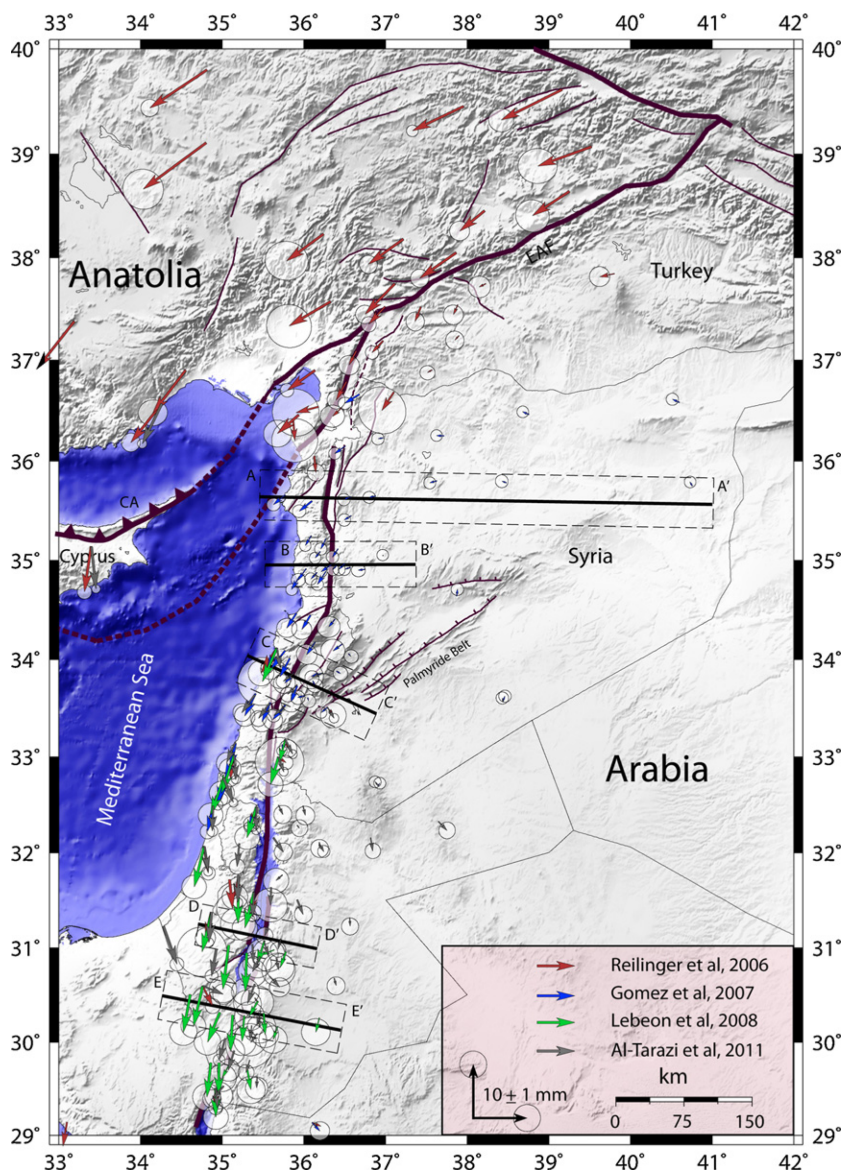

Fig. 2. (a) GPS Horizontal velocity field and the 95% confidence ellipses obtained by previous campaigns in the Eastern Mediterranean region with respect to the Arabia-fixed reference frame. GPS data are from Reilinger et al. (2006), Gomez et al. (2007) and Le Béon et al. (2008) and Al-Tarazi et al. (2011), and mapped faults from Meghraoui et al. (2011). Boxes denote the swath encompassed by the profiles shown in (b). Also shown in the map are the three major faults in the region, EAF: East Anatolian fault, DSF: Dead Sea fault, CA: Cyprus arc. (b) Plots showing the GPS velocity parallel to the Dead Sea fault in its different parts from north to south. Data are from Reilinger et al. (2006), Gomez et al. (2007) and Le Béon et al. (2008). The position of GPS points is shown relative to the Dead Sea fault which is presented as a dashed line. The plots show the predicted parallel velocities V for different elastic dislocation models (different values of slip rate and locking depth) along the fault and the decreasing of slip rate toward the north. The horizontal axe shows the distance from the fault while the vertical axe shows the velocity parallel to the fault.

Please cite this article in press as: Mahmoud, Y., et al., Kinematic study at the junction of the East Anatolian fault and the Dead Sea fault from GPS measurements. J. Geodyn. (2012), http://dx.doi.org/10.1016/j.jog.2012.05.006

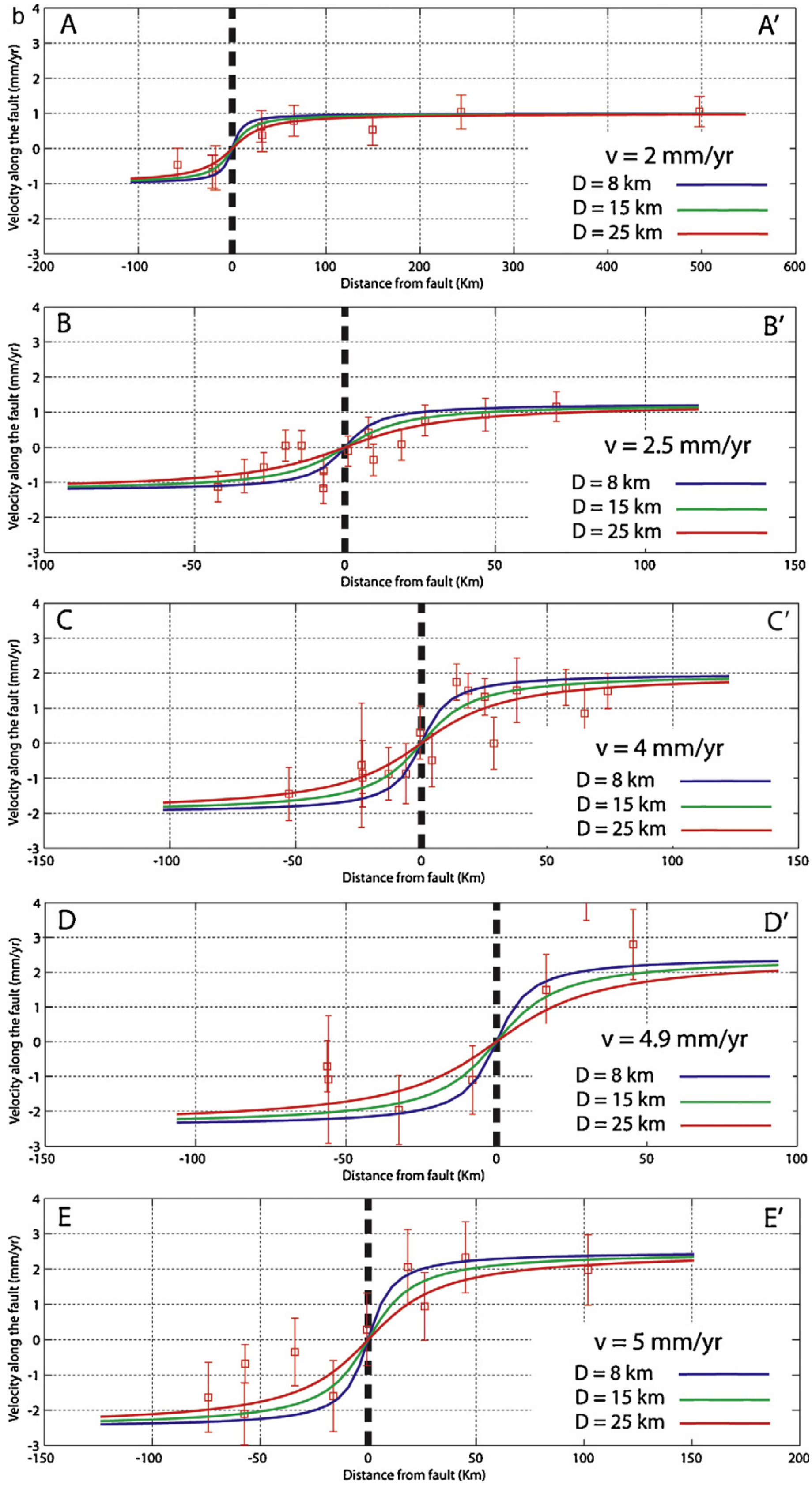

Fig. 2. (*Continued*).

related seismic activity along the Karatas-Osmaniye Fault (KOF). This is confirmed by the prominent fault scarp morphology and related active features and by the occurrence of the M_w 6.2 Adana earthquake of 1998 (Aktar et al., 2000). Furthermore, an equivalent observation can be made from the velocity vector distribution east and west of the Karasu Fault that suggests left-lateral slip with extensional component of 0.4–2.0 mm/yr along the fault. One may also observe the southward motion of SENK station located south of the Amik Basin and west of the DSF, suggesting a position on the African plate.

Unfortunately, the number of stations relative to the complex HTJ tectonics does not allow a precise determination of the individual velocity for each fault. Previous GPS studies in the eastern Mediterranean were designed for large scale tectonic issues that include the collision between the Arabian plate with Eurasia and the westward extrusion of Anatolia (Masson et al., 2007; Reilinger et al., 2006). The local tectonic complexities at the Hatay junction and the intersection between EAF, DSF and Cyprus subduction zone need a dense GPS network and detailed investigations of fault kinematics. Therefore, we developed a new GPS campaign network to densify the existing one. Moreover, the network had to be transnational in order to characterize faults which are distributed across the boundary between Turkey and Syria.

4. The new GPS network

To better characterize of the kinematic field, new GPS field campaigns were launched in southern Turkey and northern Syria. Taking into account the previous field investigations and GPS network, a new network of 4 GPS profiles across active faults and related tectonic blocks was installed and measured in 2009. The 4 GPS profiles across the Hatay region (Fig. 3) illustrate a network configuration that may contribute to an accurate estimate of the distributed tectonic activity and fault slip rate. This network contains 24 sites in Turkey and 33 sites in Syria.

The point's alignment and the continuity of the profiles from Syria to Turkey are taken into account for a better assessment of the velocity field and physical parameters of fault branches along the major fault systems. Profile 1 (E-W) crosses the Ghab basin and related north-south border faults and the NE-SW trending Lattakia

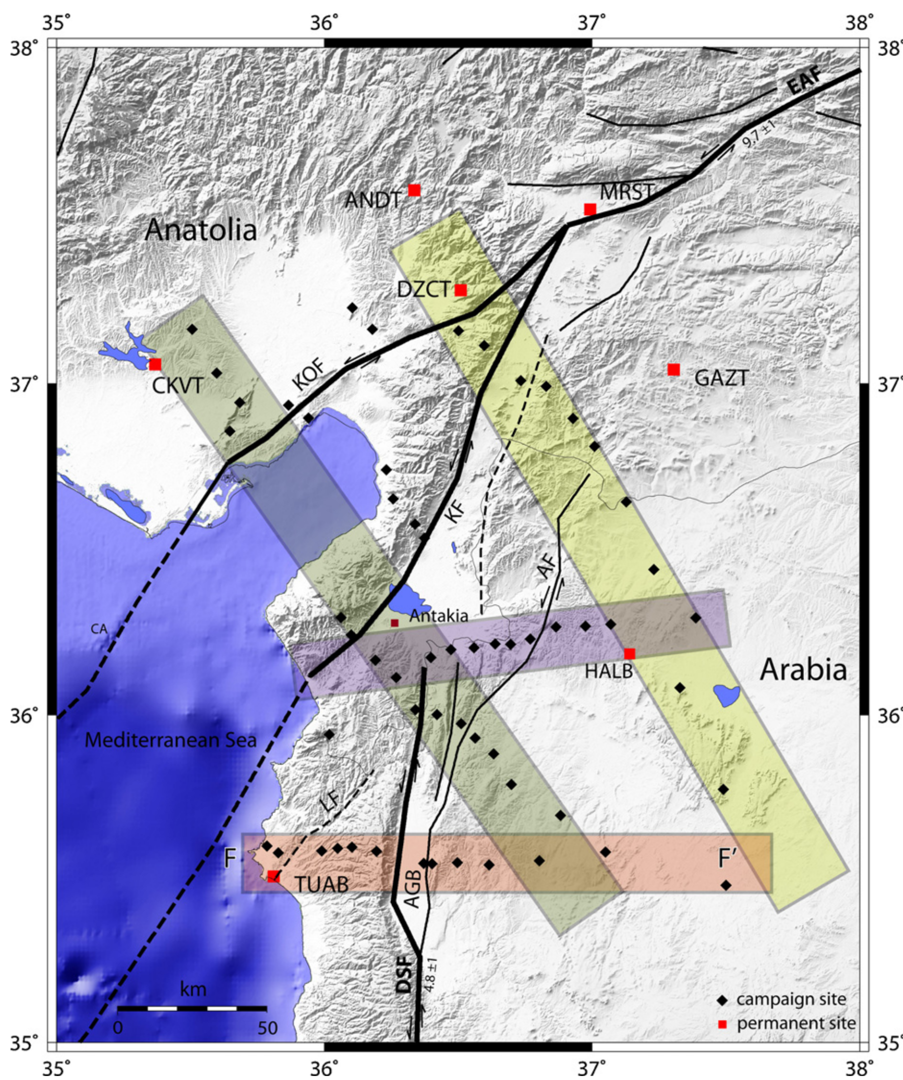

Fig. 3. New GPS network in NW Syria and SE Turkey. Black points are the campaign sites. The sites are distributed along 4 main profiles (33 points) in Syria with an extension of 2 profiles (24 points) in Turkey. The geometry of our GPS network is taken into account for a better assessment of velocity field and physical parameters of fault branches along the three major fault systems. The red points are permanent GPS stations near to the study area in Syria and Turkey. (For interpretation of the references to color in this figure legend, the reader is referred to the web version of the article.)

fault. Profile 2 crosses the easternmost fault system of the northern Ghab Basin that includes the Idleb and Afrin faults. Profile 3 (NW-SE) crosses KOF, the northern Ghab Basin and related Idleb and Afamia fault system. The Profile 4 crosses the Karasu Valley and East Anatolian fault.

As partly indicated in Fig. 3, the network is sustained by several CGPS stations in Turkey (MRST, DZCT, ANDT, CKVT, CRMT, ELZT, GAZT, MLYT) and Syria (HALB, TUAB, BUSF, RAQA, PALM, UDMC).

5. Data processing and preliminary results

The first campaign was carried out in September 2009 with the measurements of 24 points in Turkey, all sites observed for 24 h over two sessions of 12 h using Thales Z Max receivers with Thales Z Max Ashtech antenna. The 33 points in Syria were measured in October and November 2009 where each site was observed for one session of 24 h using Thales DSNP 6502MK receivers with Leica AT504 Choke Ring Antenna. The GPS data were logged with a 15 s and 30 s sampling rate in Turkey and in Syria, respectively, and antennas were fixed on monuments using antenna masts in order to minimize antenna setup errors. A second campaign took place in September and November 2010 where all the sites were measured with the same instruments and method used for the 2009 campaign. A third campaign took place in September 2011. Unfortunately, it was not be possible to measure the Syrian sites and only the Turkish side of the network has been measured three times.

The GPS data were processed together with previously collected data from a set of 8 permanent sites in Turkey and 6 others in Syria using the GAMIT/GLOBK program (Dong et al., 1998; Herring et al., 1997; King and Bock, 2000). We analyze the data in a three-step approach as described by Feigl et al. (1993) and Dong et al. (1998). In the first step, we use double difference GPS phase observations to estimate (1) the zenith delay of atmosphere at each site every 2 h, (2) the orbital and Earth orientation parameters (EOP), and (3) station coordinates for each day. We have integrated the dataset of about 50 IGS (International GPS Service) permanent stations in order to calibrate our regional observations to the global GPS network. The IGS stations cover a large domain including Africa, Eurasia and Middle East (Fig. 4) and provide daily solutions computed not only during our campaign periods but also (from January 1999 to December 2011) in order to constrain the reference frame definition. In the second step, we combine the loosely constrained parameters and their covariance in a Kalman filter to estimate a consistent set of positions and velocities. At the third step, we define the reference frame for coordinates and velocities. The horizontal velocity components have been estimated according to the International Terrestrial Reference Frame (ITRF05, Altamimi et al., 2007) using a set of 12 IGS sites as a stabilization frame (GRAS, GRAZ, JOZE, POTS, WZTR, RABT, MAS1, PDEL, BOR1, TLSE, WTZR, WSRT). Furthermore, we define an Arabia fixed reference frame minimizing the observed velocities and the velocity computed from the Arabian rotation. In Table 1 we show the Euler Pole and the angular velocities calculated in this study for Eurasia, Africa and Arabia plate and compare it with other studies (Fig. 6a,b).

In Fig. 6a and b, the preliminary velocity field obtained from the data measured in 2009, 2010 and 2011 is shown in an Eurasia and an Arabia fixed reference frame (Table 2). Our new velocity

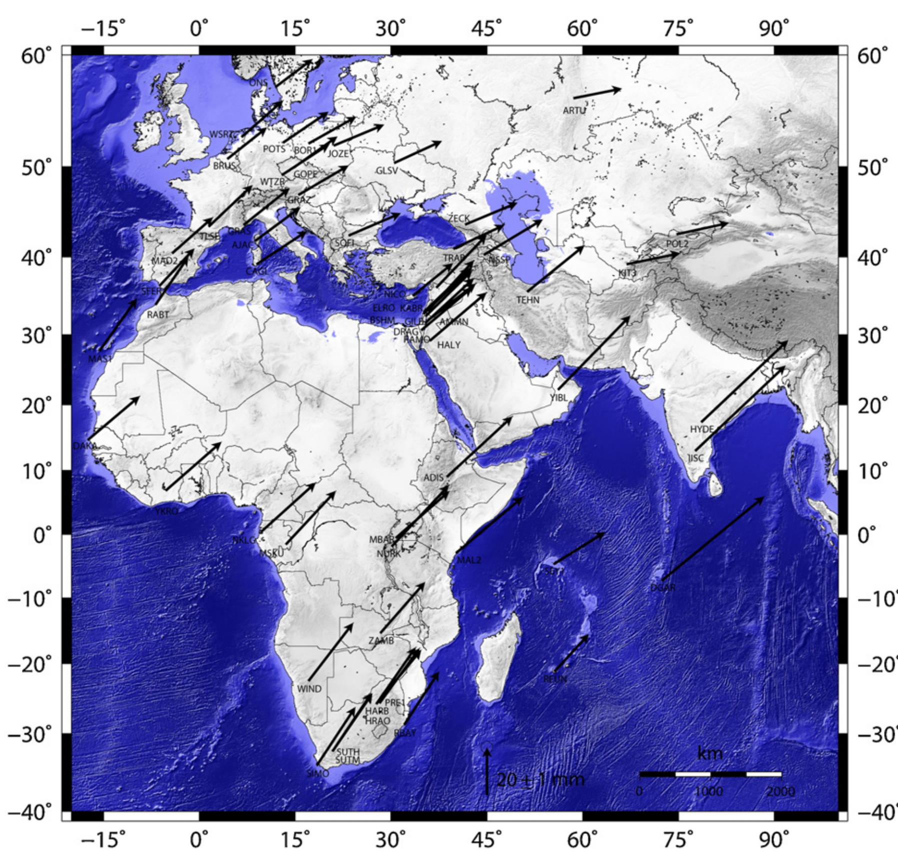

Fig. 4. GPS velocity field of the 50 IGS permanent stations used in this study to constrain our observations to the global GPS network and their 95% confidence ellipses shown in the ITRF05 reference. Data are from January 1999 to December 2010.

Please cite this article in press as: Mahmoud, Y., et al., Kinematic study at the junction of the East Anatolian fault and the Dead Sea fault from GPS measurements. J. Geodyn. (2012), http://dx.doi.org/10.1016/j.jog.2012.05.006

Table 1
The rotation pole and angular velocity for the Eurasia, Africa and Arabia plate from this study and Altamimi et al. (2007) and from the SOPAC pole rotation tables (http://sopac.ucsd.edu/cgi-bin/poleRotationValues.cgi). Solutions for Altamimi et al. (2007) and this study are relative to ITRF2005, the SOPAC solution is relative to ITRF2000.

	Lat. °N	Lon. °E	Rotation rate °/Ma
Eurasia			
This study	58.647	−100.781	0.230
Altamimi et al. (2007)	56.330	−95.979	0.261
SOPAC solution	55.851	−97.378	0.263
Africa			
This study	44.439	−79.292	0.287
Altamimi et al. (2007)	49.955	−82.501	0.269
SOPAC solution	48.997	−80.424	0.275
Arabia			
This study	49.087	6.043	0.561
Altamimi et al. (2007)	49.642	5.061	0.579
SOPAC solution	50.209	4.162	0.567

field has been also combined following the method described above, in order to be directly comparable to the previously published geodetic data of Reilinger et al. (2006) and Alchalbi et al. (2010). Due to the small time interval between the two campaigns (∼1 yr), the velocities suffer a high uncertainties. Fig. 6c shows a profile across the DSF corresponding to profile F–F′ of Fig. 3. In our point of view, only one very important conclusion can be underlined. It concerns the decreasing of the velocity of the DSF going northward and it appears that our data are consistent with 1–2 mm/yr velocity rate along the northern part of the DSF. In fact, we observe that most of the sites located west of the DSF and within the Ghab basin have velocities very small relatively to the Arabian plate. It questions the rigidity of the Sinai block in its northern end and the relationships with the Cyprus subduction zone. Effectively, the triangle located between the DSF and the Cyprus arc belonging to the Sinai block does not show significant movement relatively to Arabia. In contrast, south of Syria the Sinai block shows a significant movement relatively to the Arabia block, and hence the differential movement within the Sinai block indicate a major variation in its rigidity (Alchalbi et al., 2010).

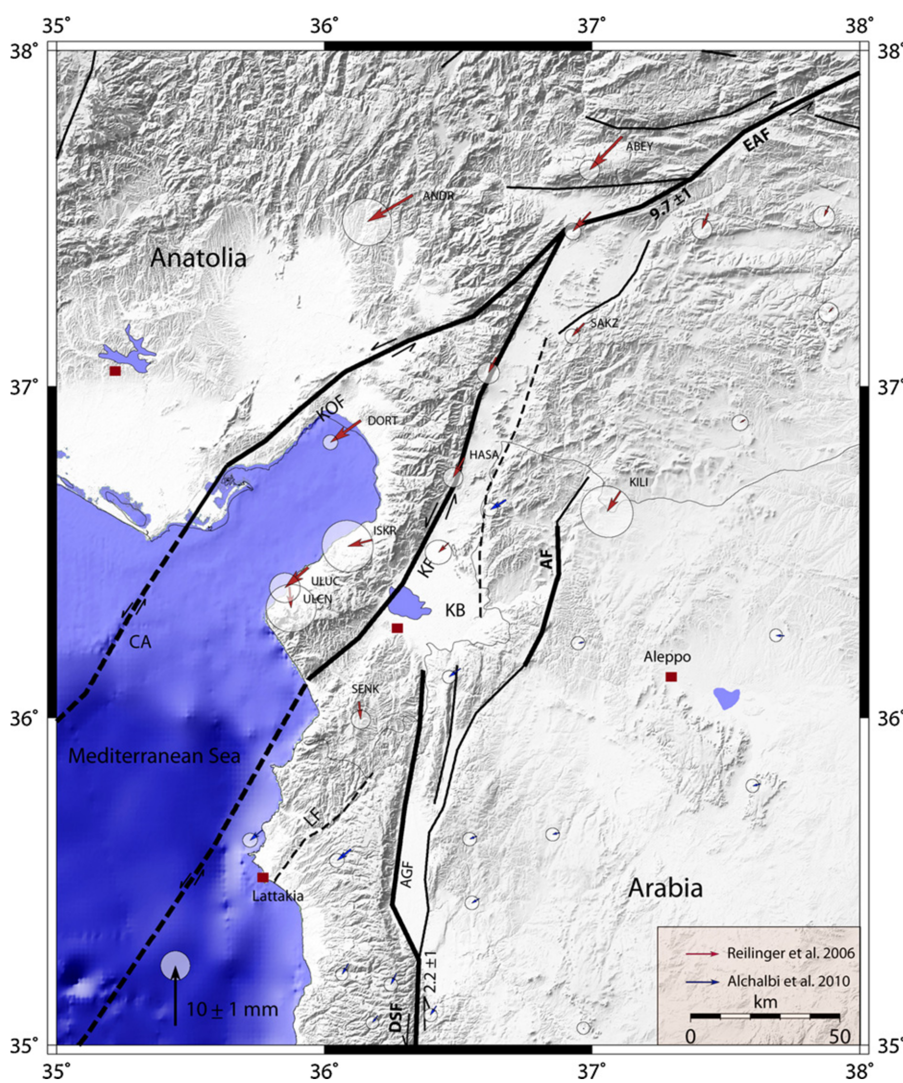

Fig. 5. GPS velocity field in the triple junction area from Reilinger et al. (2006) and Alchalbi et al. (2010) in an Arabia fixed reference frame.

Please cite this article in press as: Mahmoud, Y., et al., Kinematic study at the junction of the East Anatolian fault and the Dead Sea fault from GPS measurements. J. Geodyn. (2012), http://dx.doi.org/10.1016/j.jog.2012.05.006

Table 2
Velocities of GPS sites shown in Fig. 6b.

Site	Longitude	Latitude	Eurasia-fixed		Arabia-fixed		Sig. E	Sig. N	Corr
			Ve	Vn	Ve	Vn			
Campaign sites in Syria									
AA01	37.501	35.482	−3.32	15.43	4.61	5.79	2.33	2.51	0.035
AA02	37.051	35.583	−3.84	12.82	4.23	3.53	1.98	2.15	0.006
AA03	36.616	35.544	−4.53	7.09	3.54	−1.85	2.70	2.68	0.013
AA04	36.497	35.551	−6.80	10.79	1.29	1.95	3.48	3.61	−0.001
AA05	36.403	35.547	−4.80	16.06	3.30	7.30	3.29	3.35	−0.048
AA06	36.371	35.549	−3.76	7.65	4.34	−1.09	3.59	3.29	0.055
AA08	36.195	35.585	−7.05	3.14	1.10	−5.46	2.18	2.34	0.029
AA09	36.104	35.598	−5.30	8.72	2.87	0.20	2.54	2.73	0.054
AA10	36.050	35.595	−5.32	8.03	2.85	−0.45	1.73	1.83	−0.014
AA11	35.991	35.587	−6.35	10.84	1.81	2.41	2.72	2.78	0.011
AA12	35.828	35.581	−7.56	10.96	0.61	2.66	2.28	2.21	0.001
AA13	35.786	35.602	−9.60	7.58	−1.40	−0.69	2.83	2.82	0.033
AA14	36.803	35.557	−2.39	7.82	5.67	−1.26	3.98	4.64	−0.012
BB02	36.883	35.695	−5.65	3.33	2.53	−5.82	2.17	2.37	−0.007
BB03	36.699	35.789	−5.05	12.70	3.23	3.70	2.23	2.30	0.012
BB04	36.633	35.882	−0.23	14.48	8.14	5.53	3.52	3.45	0.051
BB05	36.564	35.931	−7.06	9.36	1.36	0.46	3.21	3.11	0.063
BB06	36.511	35.974	−3.38	5.01	5.08	−3.85	2.30	2.24	0.045
BB08	36.421	36.002	−5.40	7.33	3.10	−1.45	1.99	2.04	0.020
CC01	37.128	36.645	−14.20	−3.86	−5.20	−13.20	1.94	2.06	−0.006
CC02	37.231	36.441	−7.08	8.26	1.73	−1.17	2.52	2.84	−0.051
CC03	37.329	36.083	−5.65	9.86	2.83	0.35	1.83	2.02	0.002
CC04	37.490	35.774	−7.13	7.33	1.07	−2.30	2.38	2.74	−0.074
DD01	36.398	36.175	−5.81	8.16	2.85	−0.60	2.12	2.22	0.030
DD02	36.473	36.198	−6.51	7.95	2.16	−0.87	2.44	2.54	0.005
DD03	36.559	36.204	−2.73	4.09	5.94	−4.79	2.29	2.46	−0.010
DD04	36.638	36.216	−2.47	11.17	6.19	2.22	2.03	2.22	−0.026
DD05	36.696	36.215	−7.60	7.28	1.06	−1.72	2.06	2.27	−0.014
DD06	36.770	36.230	−5.36	7.56	3.31	−1.49	2.07	2.33	−0.014
DD07	36.866	36.267	−9.39	9.84	−0.69	0.71	2.06	2.21	−0.027
DD08	36.976	36.270	−7.31	10.30	1.37	1.08	2.07	2.14	0.019
DD09	37.070	36.275	−6.84	6.38	1.84	−2.92	2.04	2.00	−0.001
DD10	37.388	36.294	−7.08	6.61	1.59	−2.94	2.69	3.09	0.003
Campaign sites in Turkey									
PT01	35.685	36.943	−13.63	3.76	−4.24	−4.43	2.03	2.21	0.164
PT02	35.648	36.857	−12.38	7.59	−3.05	−0.56	1.87	2.07	0.086
PT04	35.866	36.935	−17.68	9.30	−8.30	0.97	1.97	2.09	0.120
PT05	35.941	36.896	−13.95	5.15	−4.62	−3.24	1.78	1.89	0.118
PT07	36.269	36.114	−5.42	9.86	3.19	1.20	1.44	1.51	0.128
PT08	36.191	36.166	−5.30	7.26	3.36	−1.33	1.37	1.45	0.120
PT09	36.341	36.017	−5.26	7.44	3.26	−1.27	1.55	1.68	0.095
PT12	36.019	35.941	−7.96	9.07	0.52	0.62	1.43	1.48	0.096
PT24	36.063	36.296	−5.48	1.97	3.32	−6.52	1.82	1.95	0.105
PT26	36.101	36.243	−7.95	7.83	0.79	−0.69	2.07	2.14	0.097
PT30	36.232	36.741	−11.98	9.70	−2.81	1.08	3.94	4.20	0.095
PT31	36.257	36.654	−10.69	7.66	−1.60	−0.99	2.10	2.19	0.113
PT33	36.339	36.577	−4.54	1.48	4.47	−7.23	1.93	2.02	0.001
PT34	36.374	36.535	−8.57	4.56	0.40	−4.18	1.90	2.01	0.065
PT35	37.009	36.812	−6.87	13.04	2.29	3.79	1.65	1.78	0.084
PT36	36.929	36.895	−8.31	10.91	0.93	1.73	1.48	1.57	0.091
PT37	36.829	36.992	−9.38	5.09	−0.04	−4.02	1.90	1.99	0.136
PT38	36.734	37.009	−9.52	6.54	−0.16	−2.49	1.89	2.01	0.055
PT39	36.598	37.114	−10.41	7.13	−0.94	−1.79	1.76	2.03	0.149
PT40	36.502	37.158	−10.05	10.39	−0.54	1.55	1.82	2.01	0.068
PT42	36.105	37.227	−16.72	2.72	−7.11	−5.81	1.76	1.87	0.094
PT43	36.179	37.162	−16.56	10.95	−7.02	2.37	1.66	1.74	0.100
PT46	35.506	37.162	−15.36	9.40	−5.75	1.36	1.74	1.80	0.118
PT47	35.599	37.031	−17.19	5.55	−7.71	−2.56	1.93	2.03	0.132
Other CGPS sites (data obtained from SOPAC and UNAVCO archives)									
AMMN	35.880	32.029	−6.34	3.22	−1.34	−5.13	0.09	0.08	−0.019
BSHM	35.023	32.779	−5.85	7.02	−0.12	−0.63	0.07	0.07	−0.054
DRAG	35.392	31.593	−5.82	6.67	−1.18	−1.28	0.01	0.01	−0.118
GILB	35.416	32.479	−6.67	6.96	−1.23	−1.01	0.07	0.07	−0.057
HALY	36.100	29.139	−2.61	8.28	−0.22	−0.24	0.08	0.07	−0.027
KABR	35.145	33.023	−6.84	6.24	−0.89	−1.51	0.08	0.08	0.021
NICO	33.396	35.141	−8.85	1.23	−0.88	−5.10	0.01	0.01	−0.133
TEHN	51.334	35.697	−3.38	10.85	2.63	−9.49	0.02	0.02	−0.073
YIBL	56.112	22.186	2.59	23.53	−3.43	−0.27	0.03	0.02	−0.079

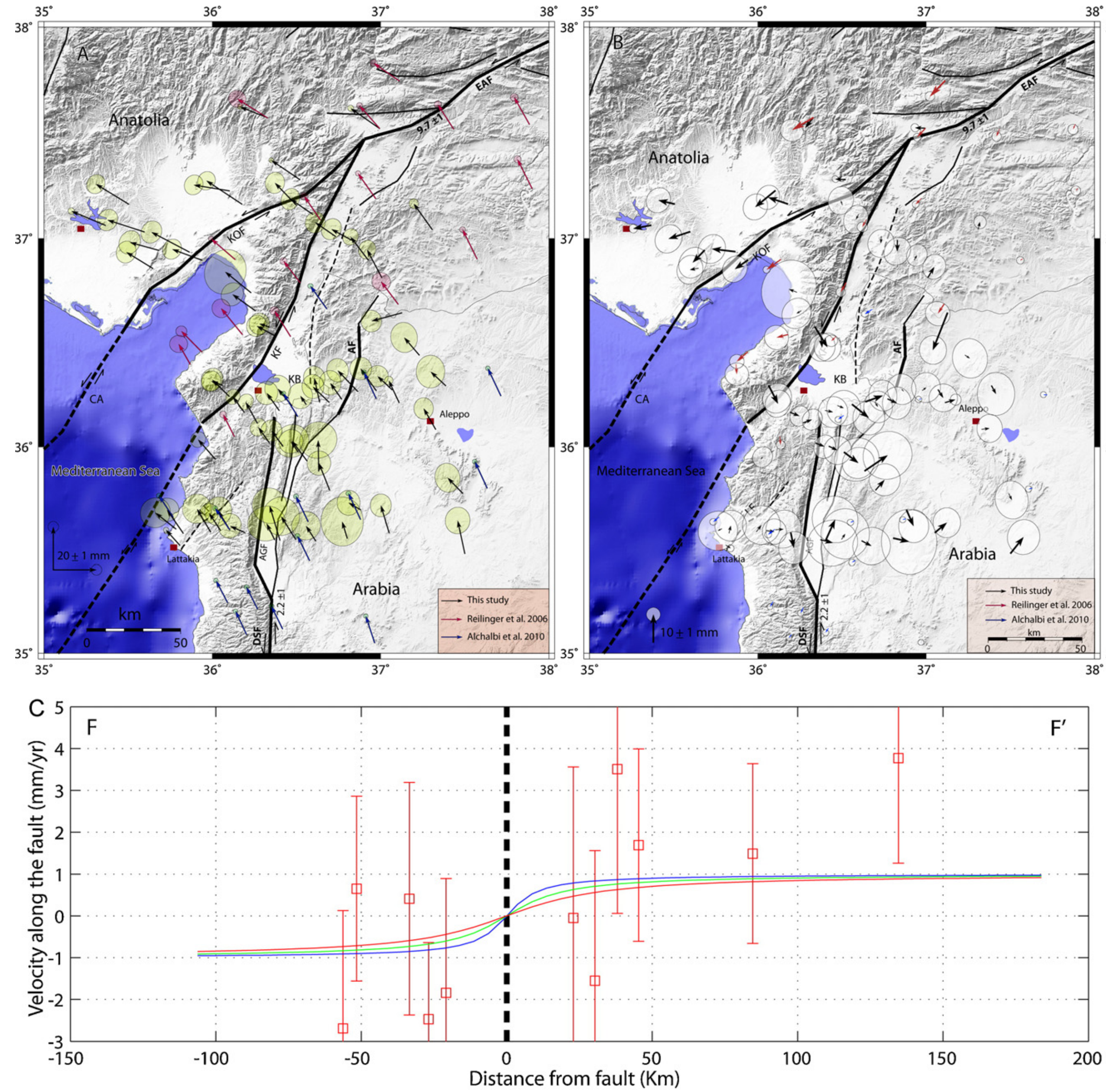

Fig. 6. (a) The GPS velocity field representing our solution for the 2009, 2010 and 2011 measurements in the Eurasia fixed reference frame. Black arrows are from this study, solutions from Reilinger et al. (2006) and Alchalbi et al. (2010) are plotted in red and blue, respectively. Fault mapping and slip rates from Meghraoui et al. (2011). Abbreviations for some key tectonic features: AGF: Al Ghab fault; AF: Afrin fault; CA: Cyprus Arc; KB: Karasu basin; KF: Karasu fault; KOF: Karatas-Osmaniye fault; LF: Lattakia fault; DSF: Dead Sea fault; EAF: East Anatolian fault. (b) The same as (a) but in the Arabia fixed reference frame. (c) The 1-D elastic dislocation models with different values of slip rate and locking depth corresponding to the profile F–F′ in Fig. 3 and the GPS velocity parallel to the fault. The plotted values are determined from the 2009 and 2010 measurements in Syria. The DSF is presented as a dashed line, the horizontal axe shows the distance from the fault while the vertical axe shows the velocity parallel to the fault. (For interpretation of the references to color in this figure legend, the reader is referred to the web version of the article.)

6. Conclusion and discussion

The GPS velocity field deduced from 2009, 2010 and 2011 campaigns for the 57 campaign sites and 14 permanent sites in the regions provides new data to describe the deformations in the HTJ and understand the tectonics of small faults. However, the campaigns are not sufficient to obtain an accurate velocity rate for most of the principal faults. Fig. 6b, does not contradict velocity rates proposed in previous studies (1–2 mm/yr across DSF, 2–3.5 mm/yr across KOF, 3–5 mm/yr across KF and 2–3 mm/yr across the AF, Gomez et al., 2007; Meghraoui et al., 2011).

The velocity vectors suffer a relative inaccuracy due to the short span time of the measurements (1 or 2 years). In general our campaign GPS velocity field vectors uncertainties are about 2.5 mm/yr for the sites in the Syrian side and about 1.5 mm/yr for the other sites in Turkey. This difference in uncertainties between sites in Turkey and Syria can be explained by the number of campaigns and the time span which are both greater in Turkey than in Syria. The CGPS sites in Turkey and Syria have better uncertainties with less than 1 mm/yr.

Despite the large uncertainties in our GPS results, we think that with further measurements, the accuracy can be improved and the profile network may help in a better understanding of the major and small fault segments tectonics and kinematics. The GPS station density and distribution in profiles perpendicular to most of fault segments in HTJ, and a longer time span of measurements will reduce the uncertainties of site velocity estimates and slip rates along faults.

References

Aktar, M., Ergin, M., Zalaybey, S., Tapirdamaz, C., Yrük, A., Biçmen, F., 2000. A lower crustal event in the northeastern Mediterranean: the 1998 Adana earthquake (M_w = 6.2) and its aftershocks. Geophysical Research Letters 27, 2361–2364.

Al-Tarazi, E., Rajab, J.A., Gomez, F., Cochran, W., Jaafar, R., Ferry, M., 2011. GPS measurements of near-field deformation along the southern Dead Sea Fault System. Geochemistry, Geophysics, Geosystems 12, Q12021.

Alchalbi, A., Daoud, M., Gomez, F., McClusky, S., Reilinger, R., Romeyeh, M.A., Alsouod, A., Yassminh, R., Ballani, B., Darawcheh, R., 2010. Crustal deformation in northwestern Arabia from GPS measurements in Syria: slow slip rate along the northern Dead Sea Fault. Geophysical Journal International 180, 125–135.

Altamimi, Z., Collilieux, X., Legrand, J., Garayt, B., Boucher, C., 2007. ITRF2005: a new release of the International Terrestrial Reference Frame based on time series of station positions and Earth Orientation Parameters. Journal of Geophysical Research 112, B09401.

Altunel, E., Meghraoui, M., Karabacak, V., Akyüz, S.H., Ferry, M., Yalçiner, C., Munschy, M., 2009. Archaeological sites (Tell and Road) offset by the Dead Sea Fault in the Amik Basin, Southern Turkey. Geophysical Journal International 179, 1313–1329.

Ambraseys, N.N., Jackson, J.A., 1998. Faulting associated with historical and recent earthquakes in the Eastern Mediterranean region. Geophysical Journal International 133, 390–406.

Ambraseys, N.N., Melville, C.P., Adams, R.D., 1994. The Seismicity of Egypt, Arabia, and the Red Sea: A Historical Review. Cambridge Univ Pr.

Daeron, M., Klinger, Y., Tapponnier, P., Elias, A., Jacques, E., Sursock, A., 2007. 12,000-year-long record of 10 to 13 paleoearthquakes on the Yammouneh Fault, Levant fault system, Lebanon. Bulletin of the Seismological Society of America 97 (3), 749–771.

Dong, D., Herring, T.A., King, R.W., 1998. Estimating regional deformation from a combination of space and terrestrial geodetic data. Journal of Geodesy 72, 200–214.

Feigl, K.L., Agnew, D.C., Bock, Y., Dong, D.N., Donnellan, A., Hager, B.H., Herring, T.A., Jackson, D.D., King, R.W., Larsen, S.K., 1993. Measurement of the velocity field in central and southern California. Journal of Geophysical Research 98, 21,677–21, 712.

Ferry, M., Meghraoui, M., Abou Karaki, N., Al-Taj, M., Khalil, L., 2011. Episodic behavior of the Jordan Valley section of the Dead Sea fault inferred from a 14-ka-long integrated catalog of large earthquakes. Bulletin of the Seismological Society of America 101, 39.

Ferry, M., Meghraoui, M., Karaki, N.A., Al-Taj, M., Amoush, H., Al-Dhaisat, S., Barjous, M., 2007. A 48-kyr-long slip rate history for the Jordan Valley segment of the Dead Sea Fault. Earth and Planetary Science Letters 260, 394–406.

Freund, R., 1970. The geometry of faulting in the Galilee. Israel Journal of Earth Sciences 19, 117–140.

Furlong, K.P., 1984. Lithospheric behavior with triple junction migration: an example based on the Mendocino triple junction. Physics of the Earth and Planetary Interiors 36, 213–223.

Ginat, H., Enzel, Y., Avni, Y., 1998. Translocated Plio-Pleistocene drainage systems along the Arava fault of the Dead Sea transform. Tectonophysics 284, 151–160.

Gomez, F., Karam, G., Khawlie, M., McClusky, S., Vernant, P., Reilinger, R., Jaafar, R., Tabet, C., Khair, K., Barazangi, M., 2007. Global Positioning System measurements of strain accumulation and slip transfer through the restraining bend along the Dead Sea fault system in Lebanon. Geophysical Journal International 168, 1021–1028.

Gomez, F., Meghraoui, M., Darkal, A.N., Hijazi, F., Mouty, M., Suleiman, Y., Sbeinati, R., Darawcheh, R., Al Ghazzi, R., Barazangi, M., 2003. Holocene faulting and earthquake recurrence along the Serghaya branch of the Dead Sea fault system in Syria and Lebanon. Geophysical Journal International 153, 658–674.

Guidoboni, E., Comastri, A., Traina, G., Phillips, B., Istituto nazionale di geofisica, 1994. Catalogue of Ancient Earthquakes in the Mediterranean Area up to the 10th Century. Istituto nazionale di geofisica, Rome.

Herring, T.A., King, R.W., McClusky, S.C., 1997. Geodetic constraints on interseismic, coseismic, and postseismic deformation in southern California. Annual Report to SCEC.

Jackson, J., McKenzie, D., 1988. The relationship between plate motions and seismic moment tensors, and the rates of active deformation in the Mediterranean and Middle East. Geophysical Journal 93, 45–73.

Karabacak, V., Altunel, E., Megraoui, M., Akyuz, h.s., 2010. Field evidences from northern Dead Sea Fault zone (South Turkey): new findings for the initiation age and slip rate. Tectonophysics 480, 172–182.

King, R.W., Bock, Y., 2000. Documentation for the MIT GPS Analysis Software: GAMIT. Massachusetts Institute of Technology, Cambridge.

Klinger, Y., Avouac, J.P., Abou Karaki, N., Dorbath, L., Bourles, D., Reyss, J.L., 2000a. Slip rate on the Dead Sea transform fault in northern Araba valley (Jordan). Geophysical Journal International 142, 755–768.

Klinger, Y., Avouac, J.P., Dorbath, L., Karaki, N.A., Tisnerat, N., 2000b. Seismic behaviour of the Dead Sea fault along Araba valley, Jordan. Geophysical Journal International 142, 769–782.

Kozhurin, A., 2007. Active faulting in the Kamchatsky Peninsula, Kamchatka-Aleutian Junction. Geophysical Monograph 172, 107–116.

Le Béon, M., Klinger, Y., Amrat, A.Q., Agnon, A., Dorbath, L., Baer, G., Ruegg, J.C., Charade, O., Mayyas, O., 2008. Slip rate and locking depth from GPS profiles across the southern Dead Sea Transform,. Journal of Geophysical Research 113, 1–19.

Mahmoud, S., Reilinger, R., McClusky, S., Vernant, P., Tealeb, A., 2005. GPS evidence for northward motion of the Sinai Block: implications for E. Mediterranean tectonics. Earth and Planetary Science Letters 238, 217–224.

Masson, F., Anvari, M., Djamour, Y., Walpersdorf, A., Tavakoli, F., Daignieres, M., Nankali, H., Van Gorp, S., 2007. Large scale velocity field and strain tensor in Iran inferred from GPS measurements: new insight for the present day deformation pattern within NE Iran. Geophysical Journal International 170, 436–440.

McKenzie, D.P., Morgan, W.J., 1969. Evolution of Triple Junctions.

Meghraoui, M., Cakir, Z., Masson, F., Mahmoud, Y., Ergintav, S., Alchalbi, A., Inan, S., Daoud, M., Yonlu, O., Altunel, E., 2011. Kinematic modelling at the triple junction between the Anatolian, Arabian, African plates (NW Syria and in SE Turkey). Geophysical Research Abstracts, vol. 13, EGU2011-12599, EGU General Assembly, Vienna 2011.

Meghraoui, M., Gomez, F., Sbeinati, R., Van der Woerd, J., Mounty, M., Darkal, A.N., Radwan, Y., Layyous, I., Al-Najjar, H., Darawcheh, R., Hijazi, F., Al-Ghazzi, R., Barazangi, M., 2003. Evidence for 830 years of seismic quiescence from palaeoseismology, archaeoseismology, and historical seismicity along the Dead Sea Fault in Syria. Earth and Planetary Science Letters 210, 35–52.

Nemer, T., Gomez, F., Al Haddad, S., Tabet, C., 2008. Coseismic growth of sedimentary basins along the Yammouneh strike slip fault (Lebanon). Geophysical Journal International 175, 1023–1039.

Niemi, T.M., Zhang, H., Atallah, M., Harrison, J.B.J., 2001. Late Pleistocene and Holocene slip rate of the northern Wadi Araba fault, Dead Sea transform, Jordan. Journal of Seismology 5, 449–474.

Papazachos, B.C., Papaioannou, C.A., 1999. Lithospheric boundaries and plate motions in the Cyprus area. Tectonophysics 308, 193–204.

Reilinger, R., McClusky, S., Vernant, P., Lawrence, S., Ergintav, S., Cakmak, R., Ozener, H., Kadirov, F., Guliev, I., Stepanyan, R., 2006. GPS constraints on continental deformation in the Africa–Arabia–Eurasia continental collision zone and implications for the dynamics of plate interactions. Journal of Geophysical Research 111.

Salamon, A., Hofstetter, A., Garfunkel, Z., Ron, H., 2003. Seismotectonics of the Sinai subplate – the eastern Mediterranean region. Geophysical Journal International 155, 149–173.

Savage, J.C., Burford, R.O., 1973. Geodetic determination of relative plate motion in central California. Journal of Geophysical Research 78, 832–845.

Sbeinati, M.R., 2010. Historical seismology, paleo-Archeoseismology and seismic hazard along the dead sea fault in Syria. Ph.D. Thesis. Strasbourg University, 332 pp.

Sbeinati, M.R., Darawcheh, R., Mouty, M., 2005. The historical earthquakes of Syria: an analysis of large and moderate earthquakes from 1365 BC to 1900 AD. Annals of Geophysics 48, 3.

Sbeinati, M.R., Meghraoui, M., Suleyman, G., Gomez, F., Grootes, P., Nadeau, M.J., Al Najjar, H., Al-Ghazzi, R., 2010. Timing of earthquake ruptures at theAl Harif Roman aqueduct (Dead Sea fault, Syria) from archaeoseismology and paleoseismology. In: Sintubin, M., Stewart, I.S., Niemi, T.M., Altunel, E. (Eds.), Special Volume Archaeoseismology and Paleoseismology. Ancient Earthquakes: Geological Society of America Special Paper 471., http://dx.doi.org/10.1130/2010.2471(20).

Zilberman, E., Amit, R., Porat, N., Enzel, Y., Avner, U., 2005. Surface ruptures induced by the devastating 1068 AD earthquake in the southern Arava valley, Dead Sea Rift, Israel. Tectonophysics 408, 79–99.

Please cite this article in press as: Mahmoud, Y., et al., Kinematic study at the junction of the East Anatolian fault and the Dead Sea fault from GPS measurements. J. Geodyn. (2012), http://dx.doi.org/10.1016/j.jog.2012.05.006